Parametric Study of Fuel Impact on Spray Behavior using High-Speed-Visualization

M. A. Reddemann*, F. Mathieu, D. Cordes, R. Kneer
Institute of Heat and Mass Transfer
RWTH Aachen University
Aachen, Germany

Abstract

In this work, fuel influence on spatial and temporal spray behavior is studied experimentally for a given Diesel-nozzle geometry. Fuels of different molecular groups with various physical and chemical properties are investigated by a parametric study. In addition to conventional Diesel, three alcohols, two alkanes, four silicon oils, two furans, two esters and one ether are used. The spray behavior of each fuel is analyzed for non-evaporating conditions utilizing fifteen different operation points with varied injection pressure and ambient density. The method of choice is high-speed visualization, providing a detailed temporal and spatial view on the spray propagation process. The spray evolution is analyzed with respect to characteristic macroscopic spray parameters such as spray cone angle, penetration length and integrated spray volume. It is found that the influence of fuel properties is reduced with increasing ambient density. An empirical correlation for the macroscopic cone angle as a function of Reynolds number and density ratio is derived and it is found that for non-evaporative ambient conditions mixture formation is mainly driven by density and viscosity. It is shown that the resulting air-fuel-ratio as the main influencing variable for resulting engine emissions is strongly influenced by fuel dependent spray behavior.

Introduction

Synthetic biomass-derived fuels with tailored properties are a promising alternative concerning the worldwide quest for new energy sources. On the one hand, their production routes can make a significant contribution to long-term sustainability of future fuels, and on the other hand, their tailor-made fuel properties offer the possibility for a significant reduction of exhaust gas emissions of today's conventional Diesel, Gasoline or Biofuels. However, the development of new synthetic fuels and their production routes requires a deep understanding of fuel influence on each single part of the combustion process. Especially mixture formation as a precondition for subsequent ignition and combustion is a key parameter with regard to the definition of an ideal synthetic fuel and therefore in the focus of this study. There are several studies in literature considering the influence of injected fuel on the behavior of sprays. Most of them consider an application-oriented comparison between Biodiesel or Biodiesel blends with Diesel, see [1], [2] or [3]. A slightly longer penetration and narrower cone angle for Biodiesel fuels compared to conventional Diesel fuel is observed. Further investigations with similar conclusions can be found in [4], [5], [6] or [7]. However, most of the studies are focused on a few fuels only, and thus a systematic analysis over a wide range of fuel properties and operation conditions is missing. Therefore, universal conclusions about the fuel influence on sprays in terms of correlations are needed. For this reason, a parametric study on fuel property influence is done in this work.

Nomenclature

D_0	nozzle outlet diameter	std_{m}	mean standard deviation
L_0	nozzle length	z	axial position
L	spray length	η	liquid viscosity
l_{min}	stoichiometric air-fuel-raio	λ	air-fuel-ratio
m	mass	ρ	liquid density
p_{a}	ambient pressure	ρ_{a}	ambient density
r	spray radius	σ	surface tension
u_0	steady outlet velocity	φ	nozzle elevation angle
T_{a}	ambient temperature	Φ	cone angle
V	spray volume		

*Corresponding author: reddemann@wsa.rwth-aachen.de

Experimental Methods

The focus of this work is on the influence of physical fuel properties or rather fuel dependent dimensionless numbers on spray behavior for Diesel configurations. Since a systematic study needs both fuels and operation points to be varied, the spray physics is analyzed using 16 fuels at 15 operation points. Such a large-scale parametric study is needed due to the fact that a fuel change always leads to a variation of many coupled parameters (e.g. density and viscosity). Table 1 shows the physical properties density ρ, viscosity η and surface tension σ, the oxygen content and the stoichiometric air-fuel-ratio (AFR) l_{min} of the fuels under consideration*. The variation of operation points is done with respect to injection pressure p_{inj}, ambient temperature T_{a}, ambient

Fuel	**Density** ρ [kg/m^3]	**Viscosity** η [x 10^{-3} Pas]	**Surf. Tension** σ [x 10^{-3} N/m]	**Oxygen Content** [%]	**Stoichiometric AFR** l_{min} [-]
THFA	1048	4.7	37.1	11.8	8.8
Ethyl-Levulinate	1004	1.9	32.5	13.6	8.1
Butyl-Levulinate	956	2.4	30.7	10.7	9.2
DMS-T10	933	9.8	20	-	-
DMS-T5	906	4.5	18	-	-
DMS-T2	887	2.5	18	-	-
DMS-T1.5	849	1.3	17	-	-
2-MTHF	841	0.4	24.6	6.3	11.2
Diesel	833	3.0	22.7	-	14.5
1-Decanol	824	10.2	28.2	3.0	13.0
1-Butanol	804	2.4	24	6.7	11.16
Ethanol	784	1.1	22	11.1	8.98
DNBE	763	0.7	22.2	3.7	12.7
n-Dodecane	744	1.4	24.8	0	15.0
iso-Octane	689	0.5	18.2	0	15.1
n-Heptane	680	0.4	19.6	0	15.1

Table 1. Physical properties of the investigated fuels at 300 K, sorted by liquid density.

pressure p_{a} or ambient density ρ_{a}, respectively. For variation of p_{inj}, a Diesel common rail injection system is used. However, conventional Diesel common rail injection systems are incapable of operating with such a fuel variety, shown above, i.e. standard tubes, filters, seals and pumps are unsuitable concerning lubricity and dissolving properties of exotic fuels. Consequently, a fuel resistant injection system was designed and used in this work, shown in Fig. 1, with both filter and backing pump removed and Teflon seals, Teflon resp. POM tubes inserted. All parts essential for spray generation remain in the system, such as the state of the art 8-hole Diesel piezo injector from BOSCH with a nozzle orifice diameter of $D_0 = 109$ µm and a length-to-diameter ratio of $L/D_0 = 9.4$. The holes are equally spaced with an elevation angle of $\varphi = 153°$. For variation of ambient con-

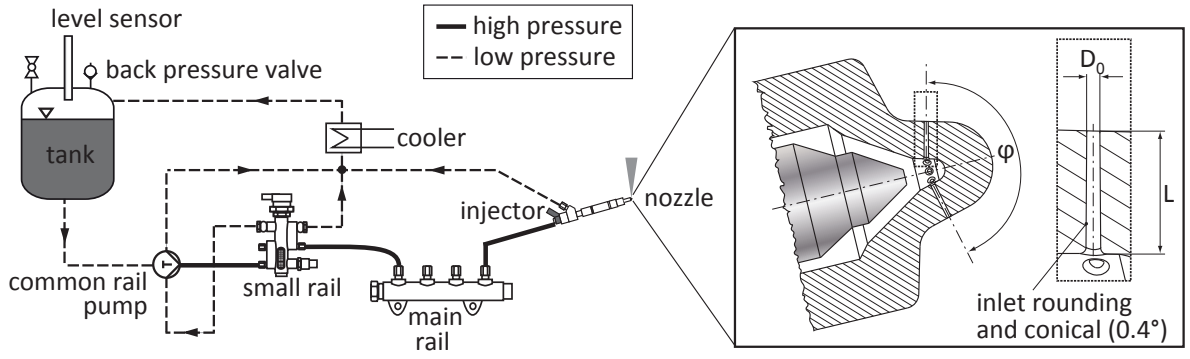

Figure 1. Fuel resistant injection system and nozzle configuration.

*DMS-TXX: DiMethylSiloxane - Trimethylsiloxy. Number indicates viscosity: XX ≙ XXcSt; 2-MTHF: 2-Methyltetrahydrofuran; THFA: Tetrahydrofurfuryl alcohol; DNBE: Di-n-butylether.

ditions an optically accessible pressurized and heated vessel is used. Such vessels allow a decoupling from the engine combustion processes and thus the investigation of spray behavior with constant and repeatable temperatures and pressures. The fifteen operating points established within vessel and injection system are shown in Tab. 2.

T K	p_a MPa	ρ_a kg/m^2	p_{inj} MPa
300	0.1	1	30, 40, 50, 60, 70
300	2.15	25	30, 40, 50, 60, 70
300	4.31	50	30, 40, 50, 60, 70

Table 2. Operating Conditions.

Macroscopic high-speed visualization is the method of choice for this parametric study, which allows the investigation of the evolution of the spray propagation process with maximum temporal and spatial resolution on the one hand and appropriate effort on the other. The experimental set-up shown in Fig. 2 is composed of a high-speed camera, a continuous light source and the aforementioned vessel. For detailed information, see Tab. 3. The injector is orientated in the vessel in such a way that one spray propagates in vertical direction. In this study this spray-cone only is investigated. Light scattered at the liquid phase is received by each image frame of the high-speed camera resulting in a consistent video of 4 ms duration and 120 frames for one single injection. For sufficient statistical accuracy 20 injection videos are recorded for each single operating condition. All diagrams in this work only show the mean values of those 20 injections. Additionally, the mean standard deviation std_m is specified inside each figure for the time interval investigated.

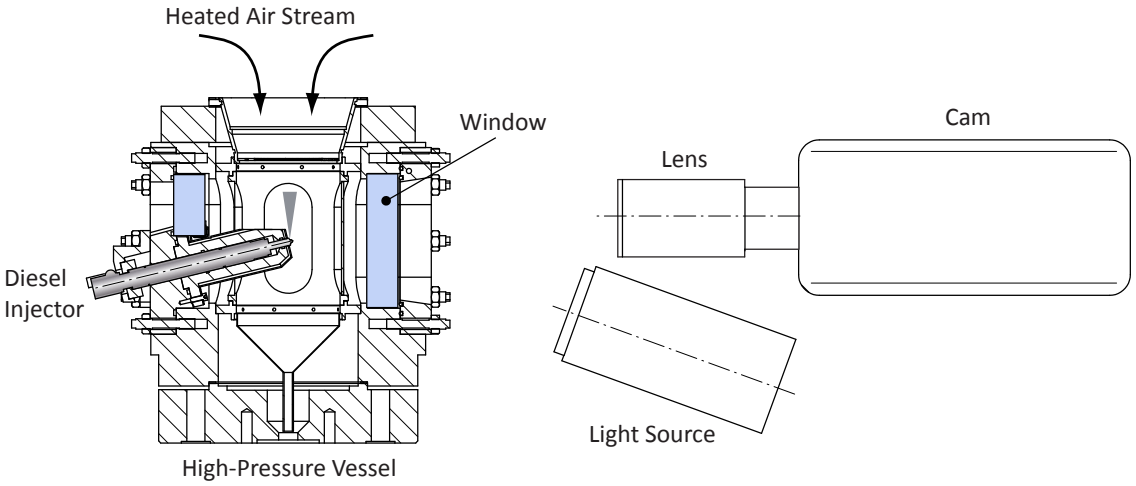

Figure 2. Optical set-up.

Light Source	***Spotlight - GK Lichttechnik GmbH***		
	Metal Halide Lamp	Osram	HTI 705 W/SE
	Power	400	W
Cam	***Photron Fastcam SA-X***		
	Recording Color Depth (greyscale)	8	bit
	Image Resolution	896x368	pixels
	Frame Rate	30.000	fps
	Pixelsize	20x20	µm^2
Lens	***Zeiss Macro-Planar T* 2/100 mm ZF***		
	Focal Length	100	mm
	Magnification Factor:	0.39	-

Table 3. Specifications of the instrumentation.

Evaluation Methods

An automatic image processing tool based on MATLAB was developed to extract information about the spray structure from greyscale images. In the first step each image is background corrected, contrast stretched and masked, followed by a binarization based on a 90% intensity threshold. These binarized images are then analyzed for each time step t with respect to geometric values such as the length $L(t)$, the cone angle $\Phi(t)$ and finally the volume $V(t)$ of the spray, see Fig. 3. Usually, the temporal evolution of spray events is described using the so called

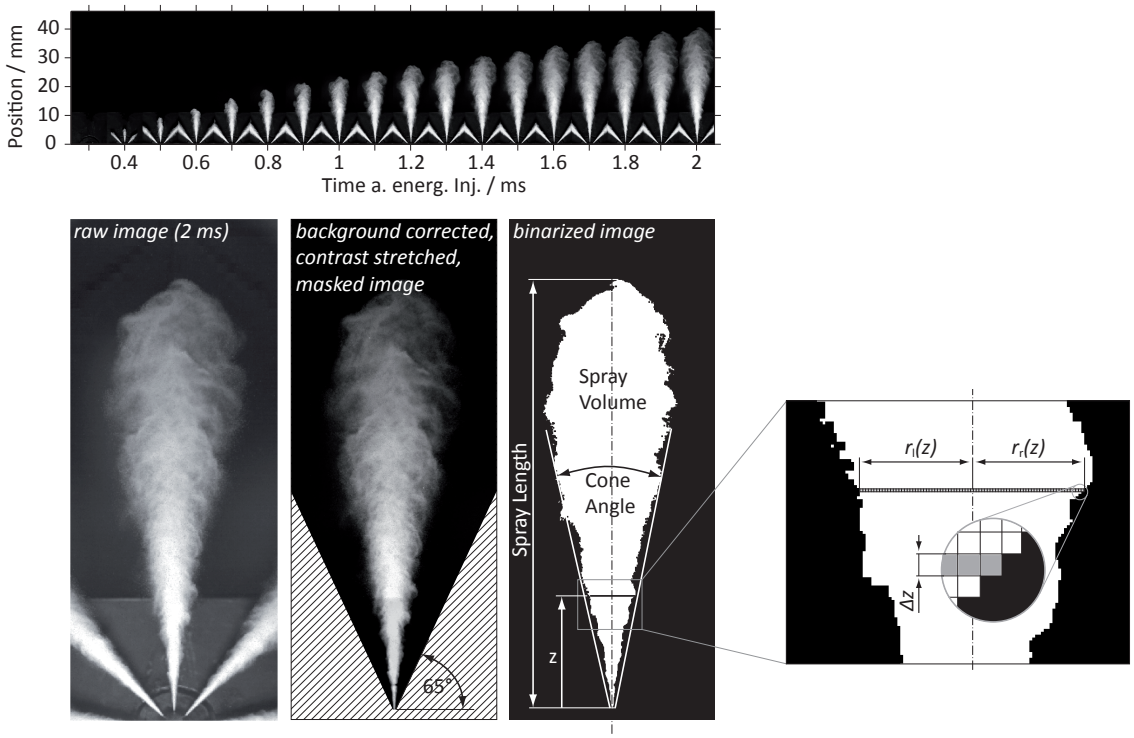

Figure 3. Measured variables.

'time after energizing the injector' t_{aei} as reference. Considering a comparison of sprays with different physical properties this time definition could lead to misinterpretations, because fuel dependent deviations in $L(t_{\text{aei}})$, $\Phi(t_{\text{aei}})$ or $V(t_{\text{aei}})$ could be enhanced or reduced by different exit delays. Since the exit delay is mainly driven by friction inside the injection system and hence by viscosity, a time definition with reference to the start of energizing could lead to an overestimation of the viscosity influence. Furthermore, the injection system is a commercial 'black box' with little information about geometry. In order to minimize this nozzle effect the reference point for time t is defined by the authors as the moment of fuel exit. This reference point must be determined for each single injection event j to encounter possible cyclic variations. It is identified in this work by the root $\tau_j = t_j(L_j = 0)$ of $L_j(t)$ and is used to correct the time after energizing $t_j = t_{\text{aei},j} - \tau_j$. In a final step the temporal evolution of each measured value of injection j such as $V_j(t_j)$ must be transferred into a reference time by linear interpolation between two neighboring values ($t_{j,k} < t < t_{j,k+1}$):

$$V_j(t) = \frac{V_j(t_{j,k+1}) - V_j(t_{j,k})}{t_{j,k+1} - t_{j,k}} \cdot (t - t_{j,k}) + V_j(t_{j,k}). \tag{1}$$

This spray volume $V_j(t)$ will now be considered in detail. For non-evaporating conditions $V_j(t)$ can be regarded as the integrated volume of injected fuel and entrained air within the determined contour until a certain time t. Assuming a rotational symmetric spray structure the complete volume of a spray can be determined as follows:

$$V_j(t) = \pi \cdot \sum_{i=1}^{N} \underbrace{\frac{1}{2} \cdot \left(r_{\text{l},i}^2 + r_{\text{r},i}^2\right)}_{\overline{r}_i^2} \cdot \Delta z \tag{2}$$

with $\overline{r}_i$ the mean spray radius at the axial distance z_i, as a function of the radii of both spray halves $r_{\mathrm{l},i}$ and $r_{\mathrm{r},i}$, as illustrated on the right of Fig. 3. $N = L/\Delta z$ is the number of circular discs of thickness Δz over the entire spray length L. The thickness $\Delta z = 51\mu$m is the height resolved by one pixel.

Results and Discussion

In Fig. 4 the liquid spray length is exemplarily shown for three different ambient conditions and one injection pressure (A similar qualitative behavior is also detectable for the remaining operation points investigated).

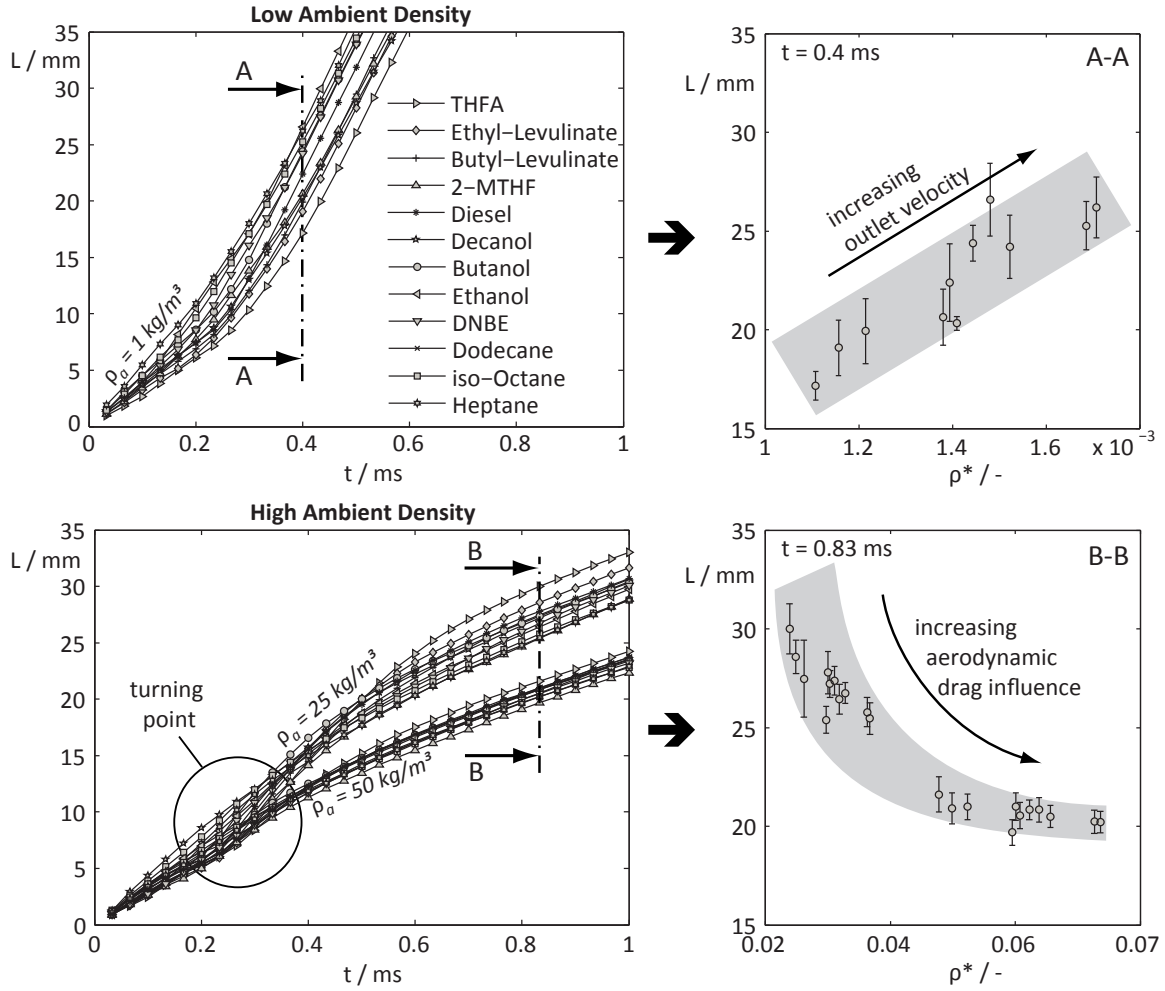

Figure 4. Left hand side: Temporal evolution of Spray Length L for twelve different fuels and three different ambient densities (above: $\rho_\mathrm{a} = 1$ kg/m^3, below: 25 kg/m^3, 50 kg/m^3) exemplarily shown for one injection pressure $p_\mathrm{inj} = 30$ MPa at non-evaporating conditions ($T_\mathrm{a} = 300$ K). Right hand side: Variation of L as a function of density ratio $\rho^* = \rho_\mathrm{a}/\rho$ for a given time step, indicated by a sectional view.

For small ambient density (1 kg/m^2) the evolution of liquid spray length L is less affected by aerodynamic drag and hence, a strong influence of the nozzle outlet condition on spray propagation is expected. Since a small liquid density results in a high outlet velocity (following the Bernoulli velocity approach: $u_0 \sim \sqrt{2\Delta p/\rho}$), fuels with small density ρ and thus high density ratio ρ^* show the longest penetration length in the region of interest, see top right of Fig. 4 (A-A).

With rising ambient density (25 kg/m^2, 50 kg/m^2) the influence of aerodynamic drag increases and as a result the penetration behavior changes significantly, see bottom left of Fig. 4. A turning point of L appears at some distance from the nozzle as a result of two fuel dependent effects: the temporal evolution of nozzle flow and the spray tip deceleration, respectively. At later times the velocity of the spray tip is fuel independent, i.e. all fuels show a parallel development of spray length with time. A closer look at this downstream region is offered by Fig. 4

at the bottom right side. Here, the fuel influence is analyzed in more detail for an exemplary time step (B-B). The density ratio is confirmed to be the main influencing variable for spray length. A larger density ratio results in a smaller spray length, contrary to the first case for low ambient density. However, the influence of the remaining fuel properties, such as viscosity and surface tension, must not be neglected: e.g. the low viscosity fuel 2-MTHF shows a shorter penetration length than expected, leading to the assumption that 2-MTHF droplets are smaller and therefore stronger decelerated. Additional droplet size measurements are needed in the future for clarification. Finally, it is found that the influence of fuel properties on spray length decreases with increasing ambient density, see bottom right. It can be concluded, that the fuel dependent momentum transfer is equalized with rising ambient density and therefore the direct and indirect droplet-droplet-interaction inside the spray. As the liquid spray length is mainly an indicator for the momentum transfer inside the spray, an analysis of the impact of fuel properties on atomization and entrainment needs additional parameters to be defined. In this work, the cone angle and the spray volume are used as indicators.

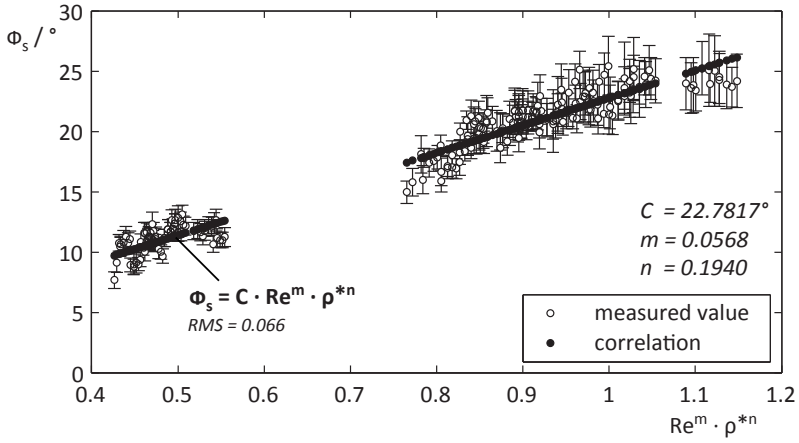

Figure 5. Cone Angle Correlation, valid for all fuels and operating conditions shown in Fig.1 and Tab. 2.

In this work the cone angle $\Phi(t)$ is determined at an axial distance of $200 \cdot D_0$ from the nozzle. For long injection durations cone angles tend to progress asymptotically towards a certain stationary value $\Phi(t \to \infty) = \Phi_\mathrm{s}$. In Fig. 5 the cone angles measured for all fuels of Tab. 1 and all operation points of Tab. 2 are shown, including the error bars resulting from averaging over twenty injections. A correlation for Φ_s developed by the authors is shown for each operation point in the same graph. It is a function of the Reynolds number Re and the density ratio $\rho^* = \rho_\mathrm{a}/\rho$ and can be written as:

$$\Phi_\mathrm{s} = C \cdot Re^m \cdot \rho^{*n} \tag{3}$$

$$\text{for} \quad 10^3 < Re < 10^5 \quad \text{and} \quad 10^{-3} < \rho^* < 0.7 \cdot 10^{-1}$$
$$\text{with} \quad C = 22.7817°, \quad m = 0.0568, \quad \text{and} \quad n = 0.1940.$$

The Reynolds number $Re = \rho D_0 u_0/\eta$ in Eq. 3 is based on an empirical approach for the outlet velocity of this nozzle u_0, derived by [8]. The RMS of this correlation is 0.0663 with a maximum relative error of 26%. Considering the fuel properties included in the dimensionless numbers the cone angle is a function of two physical parameters only, density and viscosity:

$$\Phi_s = f\left(\rho^{-0.137} \cdot \eta^{-0.0568}\right) \tag{4}$$

Thus, the surface tension which is known to be relevant for secondary breakup and subsequent droplet sizes has a negligible effect on the final cone angle. However, this does not necessarily mean that droplet sizes are fuel independent, since the visualization technique used in this work is incapable of distinguishing between different droplet sizes.

So far, only local spray parameters such as spray length L and cone angle Φ are analyzed. However, the results of both parameters should be complemented by a study of the integral measured variable volume V, as this parameter can serve as an indicator for the overall entrainment of air, see also [2]. In Fig. 6 this spray volume is illustrated for similar ambient conditions, already utilised in Fig. 4. At first sight it is obvious that

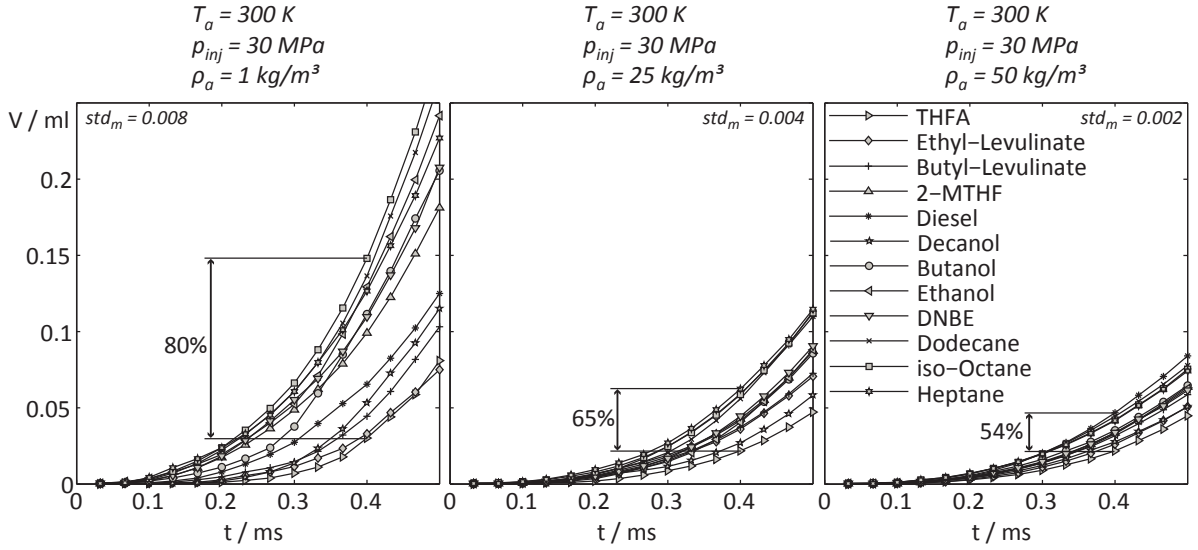

Figure 6. Fuel Influence on Spray Volume for three different ambient densities, $T_\mathrm{a} = 300$ K and $p_\mathrm{inj} = 30$ MPa.

the spray volume is much more sensitive to fuel property variations than L, although the convergence tendency for higher ambient densities is also evident here (from 80% to 54% relative deviation). It must be noticed that the spray volume is strongly influenced by the injected fuel amount, which is mainly a function of fuel density. Therefore a remarkable decrease of spray volume with increasing density is found. Furthermore, due to the integral character of V, the overall volume flow dV/dt is steadily increased i.e. contrary to other local paremters such as cone angle or spray length no turning point is detectable. Based on these results it can be concluded that air entrainment strongly depends on fuel properties (specifically fuel density).

However, for quantitative data about the fuel influence on temporal evolution of air entrainment, detailed experimental data about the temporal evolution of injection rates $\dot{m}(t)$ are favorable and will be determined in future. Alternatively, the integral injected mass can be estimated using the approach for the steady outlet velocity u_0, empirically determined by [8] and already used in Eq. 3. The steady mass flow can be written as $\dot{m}_\mathrm{s} = \pi D_0^2/4 \cdot \rho \cdot u_0$ Thus, it is assumed that the ratio of injection rates of different fuels is constant over time. By using this approach the entrained air volume flux $\dot{V}_\mathrm{a}$ can be calculated on the basis of both, overall spray volume $V(t)$ and stationary fuel mass flow $\dot{m}_\mathrm{s}$, as:

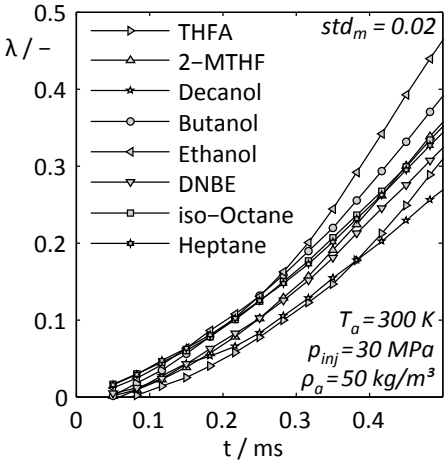

Figure 7. Fuel Influence on Air-Fuel-Ratio λ for $T_\mathrm{a} = 300$ K, $\rho_\mathrm{a} = 50$ kg/m^2 and $p_\mathrm{inj} = 30$ MPa.

$$\dot{V}_\mathrm{a}(t) = \frac{\partial V}{\partial t} - \frac{\dot{m}(t)}{\rho} \approx \frac{V_{t+\Delta t/2} - V_{t-\Delta t/2}}{\Delta t} - \frac{\dot{m}_\mathrm{s}}{\rho} \tag{5}$$

resulting in a formula for the integral air-fuel-ratio λ at time t:

$$\lambda(t) = \frac{m_\mathrm{a}(t)}{m_\mathrm{a,min}(t)} = \frac{\sum_{i=1}^{N} \rho_\mathrm{a} \cdot \dot{V}_\mathrm{a}(t) \cdot \Delta t}{\sum_{i=1}^{N} \dot{m}_\mathrm{s} \cdot l_\mathrm{min} \cdot \Delta t}. \tag{6}$$

with $N = t/\Delta t$ and $\Delta t = 1/30.000s$. In Fig. 7 the resulting temporal history of λ for nine selected fuels is

illustrated. On the assumption that a high value of λ indicates a good combustion behavior with low emissions the mixture formation performance of each fuel can be evaluated.

Even though THFA shows the smallest stoichiometric minimum air-fuel-ratio, see Tab. 1, its less air entrainment results in a worse effective air-fuel-ratio compared to the other fuels. On the other hand, Ethanol shows the maximum air-fuel-ratio of all investigated fuels, as it is characterized by a high oxygen content in combination with a good atomization and entrainment behavior. Concluding that the relevance of fuel dependent air entrainment for the subsequent air-fuel-ratio should not be underestimated, as it is most likely one determining factor for subsequent exhaust gas emissions of combustion engines.

Summary

- The fuel effect on mixture formation for different ambient densities was analyzed on the basis of spray length L and spray volume V. It was found that the sensitivity to fuel variations on macroscopic parameters is minimized with increasing aerodynamic drag.
- The liquid density was found to be the main influencing fuel property for the spray length, see Fig. 4.
- A correlation for the steady cone angle Φ_s was found and validated, cf. Eq. 3 and Fig. 5. It was shown that the cone angle mainly depends on density and viscosity. The influence of surface tension is negligible.
- On the basis of a function for the spray volume V, cf. Eq. 2, a strong dependence of V on fuel properties was found, see Fig. 6.
- The air-fuel-ratio λ was determined on the basis of an injection rate correlation and the measured spray volume V, shown in Fig. 6. It was concluded that the relevance of atomization and evaporation is as important as the oxygen content for subsequent emissions, see Fig. 7. Measurements of the injection rate in the near future will allow a more quantitative analysis of this topic.

Acknowledgements

This work was performed as part of the Cluster of Excellence "Tailor-Made Fuels from Biomass", which is funded by the Excellence Initiative of the German federal and state governments to promote science and research at German universities.

References

[1] Grimaldi, C. N. and Postrioti, L., Experimental Comparison Between Conventional and Bio derived Fuel Sprays from a Common Rail System, *SAE paper 2000-01-1252* (2000).

[2] Desantes, J. M., Payri, R., García, A. and Manin, J., Experimental Study of Biodiesel Blends Effects on Diesel Injection Processes, *Energy and Fuels*, Vol. 23, No. 3, pp.3227-3235, 2009.

[3] Deshmukh, D. and Ravikrishna, R. V., Experimental studies on high-pressure spray structure of biofuels, *Atomization and Sprays* 21(6) 467-481 (2011).

[4] Kim, H. J., Suh, H. K., Park, S. H. and Lee, C. S., An Experimental and Numerical Investigation of Atomization Characteristics of Biodiesel, Dimethyl Ether, and Biodiesel-Ethanol Blended Fuel, *Energy and Fuels* 22:2091-2098 (2008).

[5] Kim, H. J., Park, S. H., Suh, H. K. and Lee, C. S., Atomization and Evaporation Characteristics of Biodiesel and Dimethyl Ether Compared to Diesel Fuel in a High-Pressure Injection System, *Energy and Fuels* 23:1734-1742 (2009).

[6] Li, L., Zhang, X., Wu, Z., Deng, J. and Huang, C., Experimental Study of Biodiesel Spray and Combustion Characteristics, *SAE paper 2006-01-3250* (2006).

[7] Gao, J., Jiang, D. and Huang, Z., Spray properties of alternative fuels: A comparative analysis of ethanol-gasoline blends and gasoline *Fuel* 86: 1645-1650 (2007).

[8] Reddemann, M. A., Mathieu, F., Martin, D. and Kneer, R., Impact of Physical Properties on Primary Breakup for a Diesel Nozzle Configuration, *Atomization Sprays,* Vol. 21, No. 3, pp. 221-235, 2011.